Published in final edited form as:
Neuroimage. 2010 January 1; 49(1): 337–344. doi:10.1016/j.neuroimage.2009.08.009.

Dynamic *in vivo* imaging of cerebral blood flow and blood–brain barrier permeability

Ofer Prager[a,1], **Yoash Chassidim**[a,c,1], **Chen Klein**[a], **Haviv Levi**[a], **Ilan Shelef**[c], and **Alon Friedman**[a,b,*]

[a]Department of Physiology, Soroka University Medical Center and Zlotowski Center for Neuroscience, Ben-Gurion University of the Negev, Beer-Sheva, Israel

[b]Department of Neurosurgery, Soroka University Medical Center and Zlotowski Center for Neuroscience, Ben-Gurion University of the Negev, Beer-Sheva, Israel

[c]Department of Neuroradiology, Soroka University Medical Center and Zlotowski Center for Neuroscience, Ben-Gurion University of the Negev, Beer-Sheva, Israel

Abstract

The brain is characterized by an extremely rich blood supply, regulated by changes in blood vessel diameter and blood flow, depending on metabolic demands. The blood–brain barrier (BBB)—a functional and structural barrier separating the intravascular and neuropil compartments—characterizes the brain's vascular bed and is essential for normal brain functions. Disruptions to the regional cerebral blood supply, to blood drainage and to BBB properties have been described in most common neurological disorders, but there is a lack of quantitative methods for assessing blood flow dynamics and BBB permeability in small blood vessels under both physiological and pathological conditions. Here, we present a quantitative image analysis approach that allows the characterization of relative changes in the regional cerebral blood flow (rCBF) and BBB properties in small surface cortical vessels. In experiments conducted using the open window technique in rats, a fluorescent tracer was injected into the tail vein, and images of the small vessels at the surface of the cortex were taken using a fast CCD camera. Pixel-based image analysis included registration and characterization of the changes in fluorescent intensity, followed by cluster analysis. This analysis enabled the characterization of rCBF in small arterioles and venules and changes in BBB permeability. The method was implemented successfully under experimental conditions, including increased rCBF induced by neural stimulation, bile salt-induced BBB breakdown, and photothrombosis-mediated local ischemia. The new approach may be used to study changes in rCBF, neurovascular coupling and BBB permeability under normal and pathological brain conditions.

Introduction

Brain metabolism and normal function is critically dependent on proper functioning of the neurovascular unit (Iadecola, 2004). This unit comprises the cerebral circulation, including the pial and intraparenchymal cerebral blood vessels with their extrinsic and intrinsic innervation, perivascular pericytes, astrocytes and surrounding neurons. The regional

*Corresponding author. Department of Physiology, Faculty of Health Sciences, Ben-Gurion University of the Negev, Beer-Sheva 84105, Israel. Fax: +972 8 6479883. alonf@bgu.ac.il (A. Friedman).

[1]The first two authors contributed equally to the manuscript.

Appendix A. Supplementary data

Supplementary data associated with this article can be found, in the online version, at doi:10.1016/j.neuroimage.2009.08.009.

cerebral blood flow (rCBF) is related to neuronal activity and metabolic demand (also known as “neurovascular coupling,” see Baskurt and Meiselman, 2003). In addition, the rCBF is autoregulated and can therefore remain constant over a wide range of perfusion pressures (Hansen-Schwartz, 2004). Regulation of the rCBF is often impaired in pathological brain conditions associated with vascular abnormalities (e.g., stroke) and primary neuronal dysfunctions (e.g., epileptic seizure and cortical spreading depression). For example, it has been reported for both animals (Dreier et al., 1998, 2001, 2004) and human patients (Strong et al., 2007) that under specific clinical conditions (e.g., subarachnoid hemorrhage and traumatic brain injury) neurovascular coupling may be breached, leading to exacerbation of ischemic neuronal damage.

Another hallmark of vascular pathology in the brain is breakdown of the blood–brain barrier (BBB). The BBB characterizes the cerebral circulation, keeping a stable and unique extracellular environment within the neuropil, which is essential for normal neuronal functions. Clinical studies have demonstrated BBB breakdown under diverse pathological brain conditions (for review see Abbott, 2002; Neuwelt, 2004). Recent animal experiments have documented that BBB pathology may lead directly to malfunction of the neurovascular unit and hence to long-lasting changes in neuronal activity, followed by neuronal loss (Ivens et al., 2007; Seiffert et al., 2004; Tomkins et al., 2007).

Despite accumulating evidence for the role of rCBF dynamics, neurovascular coupling and BBB permeability changes in the pathogenesis of common brain diseases, there are very few methods available for the quantitative assessment of rCBF dynamics and BBB permeability in small cerebral vessels. Here we report a new dynamic imaging method for quantification of local changes in the blood flow and the permeability of small pial and surface cortical vessels under physiological and pathological conditions.

Materials and methods

All experimental procedures were approved by the Beer-Sheva Animal Ethics Committee. Chemicals were purchased from Sigma-Aldrich.

In vivo animal preparations

In vivo experiments were performed using established methods (Seiffert et al., 2004): Briefly, adult male SD rats weighing 200–300 g were deeply anesthetized by intraperitoneal injection of ketamine (100 mg/ml, 0.08 ml/100 g) and xylazine (20 mg/ml, 0.06 ml/100 g). The tail vein was catheterized, and the animal was placed in a stereotactic frame under a florescence stereomicroscope (Zeiss, SteReO Lumar V12). Body temperature was continuously monitored and maintained at 38.0 ± 0.5 °C with a heating pad. A bone window was drilled over the motor-somatosensory cortex (4 mm caudal, 2 mm frontal, 5 mm lateral to bregma) of one hemisphere. The dura was opened, and the cortex was continuously superfused with artificial cerebrospinal fluid (ACSF) containing (in mM): 129 NaCl, 21 $NaHCO_3$, 1.25 NaH_2PO_4, 1.8 $MgSO_4$, 1.6 $CaCl_2$, 3 KCl, and 10 glucose (pH 7.4). To induce increased rCBF, the intraorbital ethmoidal nerve, including the parasympathetic nerve fibers from the spheno-palatine ganglion (SPG) was isolated (Henninger and Fisher, 2007) and stimulated (NeuroPath™, BrainsGate) by two sets of 60 s of stimulation separated by an interval of 12 s (10 Hz, square pulse width 500 μs, 1–6 mA). For disruption of the BBB, the bile salt deoxycholic acid (DOC, 2 mM) was added to the ACSF (Greenwood et al., 1991; Seiffert et al., 2004), and the cortex was perfused for 30 min. To induce focal ischemia, the photochemical agent, Rose bengal (RBG; 7.5 mg/ml, in saline) was injected (0.133 ml/100 g body weight) i.v., as previously reported (Watson et al., 1985). The exposed cortex was then illuminated with a halogen light, transferred through fiber optic bundles (Zeiss, KL 1500 LCD). To confirm the generation of an infarct, after the experiment the

bone window was carefully closed, the animal was sutured and put back in cage for recovery. Two to 3 weeks later the brain was fixed by transcardial perfusion using 4% paraformaldehyde (PFA), removed and stored for 48 h in PFA (Tomkins et al., 2007). 40-μm coronal sections were mounted and stained using cresyl violet. In some experiments, animals were injected with the BBB-non-permeable albumin-binding dye Evans blue for confirmation of BBB breakdown (Rawson, 1943; Friedman et al., 1996). For method validation, in some experiments the rCBF was monitored with a laser Doppler flowmeter (LDF) (Oxford Optronix, OxyFlo™ 2000) (Dirnagl et al., 1989). Changes in the rCBF were calculated as percent change from the averaged baseline signal recorded for 30 min prior to treatment.

Real-time florescence imaging

For imaging rCBF and BBB permeability, the non-permeable florescent dye, Lucifer yellow CH dipotassium salt (LY, FW = 521.58) was injected intravenously (Easton and Fraser, 1994). Full-resolution (658×496) images of cortical surface vessels were obtained at 12–30 images/s using an EMCCD camera (Andor Technology, DL-658 M-TIL) before, during, and after injection of the tracer (total of 20–40 s). About 15–20 min after LY injection, averaged image intensity returned to pre-injection values, and the injection could be repeated.

Image analysis

To reduce memory usage and computation time, images were rescaled (to 256 × 256) using 2D bicubic interpolation (Keys, 1981). Sub-pixel image registration to overcome artifacts due to small movements was performed by applying a single step discrete Fourier transform (Guizar-Sicairos et al., 2008) to each image. To increase the signal-to-noise ratio, each frame was registered according to a moving average of several preceding images. Signal intensity changes over time and space were then analyzed. Each pixel was represented by a features vector, which was extracted from the intensity–time curve. Cluster analysis was then performed using a K-means clustering algorithm (Hartigan and Wong, 1979) to separate between signal behavior in arteries, veins and the extravascular matrix. Several physiologically relevant parameters were measured: (1) *Baseline*, representing the background intensity (“noise”) before injection of the tracer (0–2.5 s, about 30–50 images); (2) *time to incline*, time to the first detection of a significant increase in intensity compared to the baseline (tti), (3) *incline*, slope of the signal intensity increase between tti and the maximal value; (4) *time to maximal intensity* (ttmax); (5) *max*, the maximal value; and (6) *decline*, slope of the signal intensity decrease, and (7) *time to decline*, time from the tracer injection to the time at which the rapid decline terminated (*ttd*). Pixel-wise analysis maps created for each of the parameters demonstrated differences between anatomically defined arterioles, venules and extravascular brain tissue (the latter showing, as expected, a significantly smaller change in fluorescent intensity). tti, max, incline, ttmax, decline, and ttd were the features chosen for the clustering process. Automatic feature extraction from the intensity–time curve was performed by least-square errors fitting of the signal intensity curve using a segmented linear model with four segments and three internal breakpoints (Fig. 1). In the model, the middle breakpoint was set as the time to maximal intensity (the outer fixed points were the start and end points), with two degrees of freedom for the remaining two breakpoints. The two latter points achieving the minimization of the sum of squared errors (between the model and the original intensity curve) are the time to incline and time to decline points (ordered accordingly). Incline was calculated as the averaged slope of the line connecting the max value to the preceding baseline. Decline was calculated as the averaged slope from max to ttd. To calculate mean transit time (MTT), we assume that, in average, the MTT of all particles is the same and behaves approximately as a first-in-first-out sequence (Meier and Zierler, 1954). Let the times in which the first particle is entering and leaving the system be denoted as t_{enter} and t_{exit} respectively. Assuming all

particles entering the system also exit, the number of particles entering the system between t_{enter} and t_{exit} is equal to the amount of particles leaving the system after t_{exit}. Accordingly, t_{exit} is the time point which divides the total area under the intensity curve into two equal areas. Since t_{enter} = tt_inc, we can derive MTT = $t_{exit} - t_{enter}$. The number of clusters found to describe arterioles and venules were summed together as the cerebral vascular area (CBA).

Results

Direct visualization of flow in surface vessels and dynamic image analysis

Pixel-based image analysis following fluorescent tracer injection under control conditions was performed for nine animals, with LY as the tracer. On average, 5.15 ± 0.15 s after injection, the tracer was detected in the pial arterioles (Fig. 1A), followed by delayed (6.85 ± 0.30 s) labeling of the venules (Fig. 1B; for video see Supplementary material). Image analysis revealed a rapid increase, followed by a slower decrease in the intensity of the fluorescent signal, which reflected the flow of tracer through the local vasculature (Fig. 1C). Pixel-wise analysis maps created for each of the measured physiological-relevant parameters (Fig. 1D and see Methods) demonstrating differences between anatomically defined arterioles, venules and extravascular brain tissue. Indeed, cluster analysis resulted in a clear separation between blood vessels and the extravascular tissue (when the number of clusters was set to two; Fig. 1E, left) and between anatomically defined arterioles and venules (when the number of clusters was set to three; Fig. 1E, middle). Thus, the compartment identified with a shorter *tti* and a higher *incline* values was anatomically identified to inclusively include arterioles (Figs. 1A, D, left). The extravascular compartment showed, as expected, a significantly smaller change in fluorescent intensity. However, even in the presence of intact BBB (as validated histologically, see below and Seiffert et al., 2004), a small but significant increase in signal was measured (Fig. 1E “extravascular”). Signal kinetics were similar to that of the intravascular compartment, suggesting that it reflects “background” flow in blood vessels in a different focal plane. This effect was eliminated by subtracting the extravascular curve with the averaged arteriole curve (factored down according to mean maximal intensities ratio). Indeed, this resulted in a “near zero” signal change in the extravascular compartment of the intact control brain (Fig. 1E, “extravascular corrected” trace).

Imaging increased rCBF following stimulation of the ethmoidal nerve

We then explored the extent to which the method is sensitive for the detection of physiological and pathological changes in the rCBF. Previous studies demonstrated that stimulation of the ethmoidal nerve results in increased rCBF in the ipsilateral fronto-parietal cortex (Ayajiki et al., 2005; Henninger and Fisher, 2007). Repeated stimulation of the nerve by pulses greater than 1mA consistently resulted in a variable, but significant, increase in vessel diameter and in the averaged rCBF measured with LDF (n = 5, Fig. 2B). In a different set of experiments, trains of 60 s of stimulation separated by 12-s intervals (500 μs duration, 10 Hz, 1–6 mA) were given every 15 min with increasing stimulation intensity. LY was injected i.v. at the end of each train. A clear increase in vessel diameters was observed (Figs. 2A, C), with a stimulation intensity above 1 mA. Vasodilatation was greater for arterioles than for venules (data not shown). Dynamic image analysis, which was consistent with the LDF and diameter measurements, showed increased rCBF, decreased *tti* and increased *incline* and *max* values at stimulation intensities above 1mA (Figs. 2D, E). Importantly, both arterial and venous compartments showed similar responses, suggesting increased rCBF and drainage (outflow).

Imaging blood–brain barrier breakdown

The successful clustering of anatomically identified arterioles, venules and extravascular compartments via analysis of the dynamic fluorescent intensity predicted that under

conditions in which the BBB is disrupted, the impermeable tracer would diffuse out of the blood vessels and increase the image intensity in the extravascular compartment (cluster). We first tested tracer behavior before (Fig. 3A) and after (Fig. 3B) exposing the brain to DOC, a compound previously shown to cause increased BBB permeability to large molecules with no (or minimal) damage to other cellular structures (Greenwood et al., 1991; Seiffert et al., 2004). Indeed, 30 min after brain exposure to DOC, repeating tracer injection showed clear staining of the extravascular tissue (Fig. 3B; see also video 1 in the Supplementary material). This finding was confirmed by extravasation of the Evans blue–albumin complex in the brain, as was also observed after removal of the brain at the end of the experiment (Fig. 3C). Unexpectedly, LDF measurements demonstrated a steady and consistent increase in rCBF in all experiments ($n = 5$, Fig. 3D). The increased rCBF was associated with vasodilatation of both arterioles and venules (Fig. 3B); confirmed by our image analysis showing increased CBA of both the arterial and venous clusters following DOC (Fig. 3D). Vasodilatation was associated with increased *incline* and *max* values (5.4 ± 2 Units/s vs. 6.79 ± 3.6 Units/s and 594.1 ± 11.08 Units vs. 606.3 ± 27 Units for ACSF vs. DOC, respectively, $p < 0.0001$) and a decrease in the *MTT* (2.74 ± 0.97 vs. 2.15 ± 1.3 s, Figs. 3E, F), consistent with increased rCBF. In contrast to the stimulation-induced vasodilatation (Fig. 2) the increase in apparent flow in the arterial compartment following DOC was associated with a decrease in the apparent flow in the venous cluster, shown by decreased *incline* and *max* values and increased *MTT* (*incline* 3.81 ± 1.3 vs. 3.07 ± 1.5 Units/s, *max* 588.57 ± 8 vs. 572 ± 7.3 Units, and *MTT* 4.08 ± 1.02 vs. 4.84 ± 1.8 s for ACSF vs. DOC, respectively, $p<<0.001$, Figs. 3 E, F). In the extravascular compartment (cluster), the response to DOC was manifested mainly characterized by a late and persistant increase in intensity reflecting the accumulation of tracer in the extravascular compartment (Fig. 3F). Overall, the data suggest that DOC induces vasodilatation, increased flow in brain arterioles and increase BBB permeability leading to the accumulation of tracer in the extravascular space, which probably underlies the decreased signal in the venous compartment.

Imaging blood flow in experimental focal ischemia

To implement our imaging and analysis methods for conditions in which blood flow is reduced, we used the RBG model to induce focal intravascular thrombosis. Thirty minutes after i.v. injection of RBG and exposure to light, repeated LY injection demonstrated a clear focal reduction in rCBF (“center” in Fig. 4B; see also video 2 in the Supplementary material). As expected, image intensity changes in both the arterial and venous compartments were significantly reduced (Fig. 4D). The resultant ischemia was confirmed by histological studies showing a large necrotic lesion and loss of cortical tissue three weeks after treatment (Fig. 4D). Interestingly, In the region surrounding the ischemic area (“surround” in Fig. 4B), increased *incline* and *max* values were observed in both arterial and venous compartments (Figs. 4C, D). Importantly, the extravascular compartment showed a delayed increase in intensity (and apparent slowing of the *decline* phase), similar to that observed when the BBB was disrupted (Fig. 3). This finding was supported by extravasation of the Evans blue–albumin complex into the brain tissue surrounding the treated cortex (Fig. 4D).

Discussion

The importance of measuring dynamic changes in the rCBF and in BBB properties *in vivo* lies in the complex interactions between different components of the neurovascular unit and the dynamic nature of the unit during both physiological and pathological activation. Here, we describe a new direct imaging method for *in vivo* detection of BBB breakdown and relative CBF changes under normal and pathological conditions. The method combines real-time fluorescence imaging of small cortical vessels with quantitative image analysis using

in-house tailored MATLAB-scripts. Our method thus fuses recently described techniques based on fluorescent tracers and *in vivo* microscopy (e.g. Murphy et al., 2008; Nishimura et al., 2006) to facilitate high-resolution dynamic brain imaging. To the best of our knowledge, our technology constitutes the first quantitative approach for evaluation of rCBF and BBB permeability by using high-resolution imaging combined with powerful image analysis approaches. In this study, we demonstrated that the method facilitates: (1) reliable distinction between arterioles, venules and extravascular compartments; (2) the observation of relatively small changes in rCBF in response to neuronal stimulation; (3) the detection of altered BBB permeability in vivo; and (4) the detection of regional changes in rCBF (e.g., ischemic center and surrounding tissue, arterial and venous parts of the brain circulation).

Regional blood flow within the brain is tightly controlled by autoregulatory mechanisms and by the brain's metabolic demands (for review see Hansen-Schwartz, 2004; Strandgaard and Paulson, 1984). Most neurological disorders are associated with impaired blood supply, i.e., a decrease (e.g., stroke) or increase (e.g., seizures) in rCBF and in some cases with abnormally regulated rCBF (Dreier et al., 2000; Strong et al., 2007). The complex nature of changes in blood flow and their relation to the pathogenesis of brain diseases calls for dynamic high-resolution methods for monitoring rCBF. The various methods used in previous studies to investigate dynamic changes in rCBF include LDF (Dirnagl et al., 1989) and thermal diffusion flowmetry (TDF) (Bhatia and Gupta, 2007). Although LDF can provide instantaneous, continuous and real-time measurements of relative changes in rCBF, its drawbacks are limited spatial resolution and inability to differentiate between arterial and venous compartments or report changes in BBB permeability. TDF, which is based on thermal conductivity of the cortical tissue, provides continuous real-time assessment of rCBF changes. However, TDF is an invasive method and similarly to LDF measurements are relative in nature (Bhatia and Gupta, 2007). Among the noninvasive methods that are available today to study dynamic changes in rCBF are those based on near infrared spectroscopy (NIRS), positron emission tomography (PET), and magnetic resonance imaging (MRI). NIRS, which gives a measure of blood volume and blood oxygenation levels (Rovati et al., 2007), can be used to measure the oxygenated hemoglobin concentrations as an index of rCBF in a continuous and non-invasive manner. The drawbacks of this method are cortical-limited measurements and low spatial resolution (Shibasaki, 2008). PET has limited use since it suffers from poor spatial resolution and the need for radioactive tracers (Ishiwata et al., 2008). MRI, in its commonly used form, gives fine anatomical details of the human brain (Hacke et al., 2005; Leithner et al., 2008) but does not give a dynamic functional picture. In addition, continuous, prolonged monitoring with this technology cannot be done in most patients and centers.

BBB breakdown is associated with numerous brain pathologies such as ischemia, stroke, trauma, brain tumors and epilepsy (for review, see Ballabh et al., 2004; Neuwelt, 2004; Abbott et al., 2006), and has recently been linked directly to the pathogenesis of neuronal dysfunction and degeneration (Ivens et al., 2007; Seiffert et al., 2004; Tomkins et al., 2007; Zlokovic, 2008). Thus, measurements of changes in vessel permeability, in terms of extent and timing, may be crucial for our understanding of the pathophysiology of brain diseases. To date, BBB breakdown is most commonly evaluated by traditional “static”, usually semi-quantitative methods, in which BBB non-permeable dyes or fluorescent tracers, such as Evans blue (Ehrlich, 1885; Rawson, 1943; Friedman et al., 1996; Seiffert et al., 2004) or Nafluorescein (Hartl et al., 1997; Lenzser et al., 2007), are injected into the periphery and detected within the brain parenchyma. Immunostaining can also be used to detect blood-borne proteins within the brain [e.g., against serum albumin or immunoglobulins (Rigau et al., 2007; van Vliet et al., 2007)]. An alternative approach sometimes used in the clinical setting is the detection of brain-borne proteins (e.g., S100) within the blood (Marchi et al., 2003).While these approaches give a semi-quantitative assessment for a single time point,

they do not enable a more dynamic measurement of changes in the extent of BBB breakdown in time and space.

Various *in vivo* approaches—some static and others more dynamic—have been developed for animal studies and for human diagnostics using NIRS (Klohs et al., 2009), computerized tomography (Bisdas et al., 2008; Tomkins et al., 2001) and MRI (Neumann-Haefelin et al., 2000; Stoll et al., 2008; Tofts et al., 1999; Tomkins et al., 2008). While some of these methods have the advantages of full brain imaging and often the ability for repeated measurements in a single animal, they are limited in terms of their low signal-to-noise ratio and spatial resolution and the limited number of contrast agents available. However, some of the computational and modeling approaches developed for dynamic contrast-enhanced imaging (e.g. Tofts et al., 1999) could be implemented in the future on the data obtained by the method presented in the present manuscript. NIRS has also been recently used successfully to evaluate relative changes in BBB permeability in the cortical surface (Klohs et al., 2009). An alternative technique to study BBB permeability is by measuring the transendothelial electrical resistance (Butt et al., 1990; Crone and Christensen, 1981). However, this approach is invasive, technically challenging and is limited in its ability for repeated measures at different brain regions. The method presented here is, to the best of our knowledge, the first to combine real-time imaging of changes in BBB permeability with rCBF. The use of tracers with a short half life in the circulation facilitates repeated scans and dynamic studies (e.g., Figs. 2–4). In addition, the use of tracers with different molecular structures is expected to improve our understanding of BBB properties under disease conditions. In this study, we used a stereomicroscope, thus limiting our measurements to surface cortical vessels. Although these vessels appear to share many morphological and functional features with the deeper intracerebral microcirculation, including ultrastructural characteristics, permeability of cell junctions, trans-EC electrical resistance, there are also important differences between them, including the heterogeneous expression of some tight junction proteins (Allt and Lawrenson, 1997) and their proximity to the astrocytic glia limitants. We confirmed—using a well-established BBB disruption procedure (exposure to bile salts)—that surface vessels show a clear increase in permeability, reflecting similar changes to those reported for deeper vessels (Fig. 3; Greenwood et al., 1991; Seiffert et al., 2004). The use of two-photon microscopy (Shih et al., 2009; Stefanovic et al., 2007) will enable implementation of the analysis methods developed in the present study to deeper vessels. This limitation seems also to underlie the small change we observed in the extravascular compartment in the healthy brain. To overcome this potential limitation we assumed that the “background” intensity change (results of blood flow in adjacent focal plans) is similar to that in the arterial compartment reduced by a factor. Indeed, such correction resulted in a “near zero” intensity changes in the intact brain, with no effect on detection of the delayed increase in signal intensity observed under BBB breakdown (Figs. 3–4).

A significant question for any method is how sensitive it is for the detection of changes under both physiological and pathological conditions. We showed that neuronal stimulation resulting in vasodilatation of 10–20% of the vessel diameter induced increased rCBF, which was clearly detected using our method. In a model for focal intravascular ischemia, we could distinguish between core ischemic lesions and the surrounding brain tissue supplied by neighboring vessels (<0.5 mm distance, see Fig. 4). Although this surrounding brain region had an intact blood supply, it showed increased perfusion and increased BBB permeability, as has been described for the penumbra region.

An obvious limitation of our method is that it requires the use of the open window technique, which limits its application to anaesthetized experimental animals. However, recent developments have already made it possible to conduct prolonged experiments and to

obtain repeated measurements from animals with cranial windows (Seylaz et al., 1999; Tomita et al., 2005). The use of similar approaches in selected surgical patients or in a microcirculation system that is more accessible (i.e., retinal vessels) may well be adopted in the future to assess blood flow and permeability, and thus improve diagnosis and monitoring.

In conclusion, the presented method offers a new tool to study dynamic, regional blood flow changes in small and specific vessels together with changes in BBB properties. The method may serve as a powerful tool for improving our understanding of disease mechanisms and different therapeutic modalities.

Supplementary Material

Refer to Web version on PubMed Central for supplementary material.

Acknowledgments

Supported by the Sonderforschungsbereich TR3, the Israel Science Foundation (566/07), the Binational US-Israel Foundation (BSF 2007185) and Brainsgate.

References

Abbott NJ. Astrocyte-endothelial interactions and blood–rain barrier permeability. J. Anat. 2002; 200:629–638. [PubMed: 12162730]

Abbott NJ, Ronnback L, Hansson E. Astrocyte-endothelial interactions at the blood–brain barrier. Nat. Rev. Neurosci. 2006; 7:41–53. [PubMed: 16371949]

Allt G, Lawrenson JG. Is the pial microvessel a good model for blood–brain barrier studies? Brain Res. Rev. 1997; 24:67–76. [PubMed: 9233542]

Ayajiki K, Fujioka H, Shinozaki K, Okamura T. Effects of capsaicin and nitric oxide synthase inhibitor on increase in cerebral blood flow induced by sensory and parasympathetic nerve stimulation in the rat. J. Appl. Physiol. 2005; 98:1792–1798. [PubMed: 15626754]

Ballabh P, Braun A, Nedergaard M. The blood–brain barrier: an overview: structure, regulation, and clinical implications. Neurobiol. Dis. 2004; 16:1–13. [PubMed: 15207256]

Baskurt OK, Meiselman HJ. Blood rheology and hemodynamics. Semin. Thromb. Hemost. 2003; 29:435–450. [PubMed: 14631543]

Bhatia A, Gupta A. Neuromonitoring in the intensive care unit. II. Cerebral oxygenation monitoring and microdialysis. Intensive Care Med. 2007; 33:1322–1328. [PubMed: 17522846]

Bisdas S, Yang X, Lim C, Vogl T, Koh T. Delineation and segmentation of cerebral tumors by mapping blood–brain barrier disruption with dynamic contrast-enhanced CT and tracer kinetics modeling—a feasibility study. Eur. Radiol. 2008; 18:143–151. [PubMed: 17701183]

Butt AM, Jones HC, Abbott NJ. Electrical resistance across the blood–brain barrier in anaesthetized rats: a developmental study. J. Physiol. 1990; 429:47–62. [PubMed: 2277354]

Crone C, Christensen O. Electrical resistance of a capillary endothelium. J. Gen. Physiol. 1981; 77:349–371. [PubMed: 7241087]

Dirnagl U, Kaplan B, Jacewicz M, Pulsinelli W. Continuous measurement of cerebral cortical blood flow by laser-Doppler flowmetry in a rat stroke model. J. Cereb. Blood Flow Metab. 1989; 9:589–596. [PubMed: 2674168]

Dreier JP, Korner K, Ebert N, Gorner A, Rubin I, Back T, Lindauer U, Wolf T, Villringer A, Einhaupl KM, Lauritzen M, Dirnagl U. Nitric oxide scavenging by hemoglobin or nitric oxide synthase inhibition by N-nitro-l-arginine induces cortical spreading ischemia when K+ is increased in the subarachnoid space. J. Cereb. Blood Flow Metab. 1998; 18:978–990. [PubMed: 9740101]

Dreier JP, Ebert N, Priller J, Megow D, Lindauer U, Klee R, Reuter U, Imai Y, Einhaupl KM, Victorov I, Dirnagl U. Products of hemolysis in the subarachnoid space inducing spreading

ischemia in the cortex and focal necrosis in rats: a model for delayed ischemic neurological deficits after subarachnoid hemorrhage? J. Neurosurg. 2000; 93:658–666. [PubMed: 11014545]

Dreier JP, Petzold G, Tille K, Lindauer U, Arnold G, Heinemann U, Einhaupl KM, Dirnagl U. Ischaemia triggered by spreading neuronal activation is inhibited by vasodilators in rats. J. Physiol. 2001; 531:515–526. [PubMed: 11230523]

Dreier JP, Tille K, Dirnagl U. Partial antagonistic effect of adenosine on inverse coupling between spreading neuronal activation and cerebral blood flow in rats. Neurocrit. Care. 2004; 1:85–94. [PubMed: 16174901]

Easton AS, Fraser PA. Variable restriction of albumin diffusion across inflamed cerebral microvessels of the anaesthetized rat. J. Physiol. Online. 1994; 475:147–157.

Ehrlich P. Das Sauerstoffbeduerfnis des Organismus: Eine Farbenanalytiche Studie. Hirschwald. 1885; 8:167.

Friedman A, Kaufer D, Shemer J, Hendler I, Soreq H, Tur-Kaspa I. Pyridostigmine brain penetration under stress enhances neuronal excitability and induces early immediate transcriptional response. Nat. Med. 1996; 2:1382–1385. [PubMed: 8946841]

Greenwood J, Adu J, Davey AJ, Abbott NJ, Bradbury MW. The effect of bile salts on the permeability and ultrastructure of the perfused, energy-depleted, rat blood–brain barrier. J. Cereb. Blood Flow Metab. 1991; 11:644–654. [PubMed: 2050752]

Guizar-Sicairos M, Thurman ST, Fienup JR. Efficient subpixel image registration algorithms. Optical Lett. 2008; 33:156–158.

Hacke W, Albers G, Al-Rawi Y, Bogousslavsky J, Davalos A, Eliasziw M, Fischer M, Furlan A, Kaste M, Lees KR, Soehngen M, Warach S. for The DIAS Study Group. The Desmoteplase in Acute Ischemic Stroke Trial (DIAS): a phase II MRI-based 9-hour window acute stroke thrombolysis trial with intravenous desmoteplase. Stroke. 2005; 36:66–73. [PubMed: 15569863]

Hansen-Schwartz J. Cerebral vasospasm: a consideration of the various mechanisms involved in the pathophysiology. Neurocrit. Care. 2004; 1:235–246. [PubMed: 16174921]

Hartigan A, Wong MA. A K-means clustering algorithm. Applied Statistics. 1979; 28:100–108.

Hartl R, Medary MB, Ruge M, Arfors KE, Ghajar J. Early white blood cell dynamics after traumatic brain injury: effects on the cerebral microcirculation. J. Cereb. Blood Flow Metab. 1997; 17:1210–1220. [PubMed: 9390653]

Henninger N, Fisher M. Stimulating circle of Willis nerve fibers preserves the diffusion-perfusion mismatch in experimental stroke. Stroke. 2007; 38:2779–2786. [PubMed: 17761922]

Iadecola C. Neurovascular regulation in the normal brain and in Alzheimer's disease. Nat. Rev. Neurosci. 2004; 5:347–360. [PubMed: 15100718]

Ishiwata K, Ishii K, Kimura Y, Kawamura K, Oda K, Sasaki T, Sakata M, Senda M. Successive positron emission tomography measurement of cerebral blood flow and neuroreceptors in the human brain: an 11C-SA4503 study. Ann. Nucl. Med. 2008; 22:411–416. [PubMed: 18600419]

Ivens S, Kaufer D, Flores LP, Bechmann I, Zumsteg D, Tomkins O, Seiffert E, Heinemann U, Friedman A. TGF-beta receptor-mediated albumin uptake into astrocytes is involved in neocortical epileptogenesis. Brain. 2007; 130:535–547. [PubMed: 17121744]

Keys RG. Cubic convolution interpolation for digital image. IEEE transactions on acoustics, speech, and signal processing. 1981:29.

Klohs J, Steinbrink J, Bourayou R, Mueller S, Cordell R, Licha K, Schirner M, Dirnagl U, Lindauer U, Wunder A. Near-infrared fluorescence imaging with fluorescently labeled albumin: a novel method for non-invasive optical imaging of blood–brain barrier impairment after focal cerebral ischemia in mice. J. Neurosci. Methods. 2009; 180:126–132. [PubMed: 19427539]

Leithner C, Gertz K, Schr÷ck H, Priller J, Prass K, Steinbrink J, Villringer A, Endres M, Lindauer U, Dirnagl U, Royl G. A flow sensitive alternating inversion recovery (FAIR)-MRI protocol to measure hemispheric cerebral blood flow in a mouse stroke model. Exp. Neurol. 2008; 210:118–127. [PubMed: 18037417]

Lenzser G, Kis B, Snipes JA, Gaspar T, Sandor P, Komjati K, Szabo C, Busija DW. Contribution of poly(ADP-ribose) polymerase to postischemic blood–brain barrier damage in rats. J. Cereb. Blood Flow Metab. 2007; 27:1318–1326. [PubMed: 17213862]

Marchi N, Rasmussen P, Kapural M, Fazio V, Kight K, Mayberg MR, Kanner A, Ayumar B, Albensi B, Cavaglia M, Janigro D. Peripheral markers of brain damage and blood–brain barrier dysfunction. Restor. Neurol. Neurosci. 2003; 21:109–121. [PubMed: 14530574]

Meier P, Zierler KL. On the theory of the indicator-dilution method for measurement of blood flow and volume. J. Appl. Physiol. 1954; 6:731–744. [PubMed: 13174454]

Murphy TH, Li P, Betts K, Liu R. Two-photon imaging of stroke onset in vivo reveals that NMDA-receptor independent ischemic depolarization is the major cause of rapid reversible damage to dendrites and spines. J Neurosci. 2008; 28:1756–1772. [PubMed: 18272696]

Neumann-Haefelin T, Kastrup A, de Crespigny A, Yenari MA, Ringer T, Sun GH, Moseley ME, Fisher M. Serial MRI after transient focal cerebral ischemia in rats: dynamics of tissue injury, blood–brain barrier damage, and edema formation. Stroke. 2000; 31:1965–1973. [PubMed: 10926965]

Neuwelt EA. Mechanisms of disease: the blood–brain barrier. Neurosurgery. 2004; 54:131–140. [PubMed: 14683550]

Nishimura N, Schaffer CB, Friedman B, Tsai PS, Lyden PD, Kleinfeld D. Targeted insult to subsurface cortical blood vessels using ultrashort laser pulses: three models of stroke. Nat. Meth. 2006; 3:99–108.

Rawson RA. The binding of T-824 and structurally related diazo dyes by plasma proteins. Am. J. Physiol. 1943; 138:708–717.

Rigau V, Morin M, Rousset MC, de BF, Lebrun A, Coubes P, Picot MC, Baldy-Moulinier M, Bockaert J, Crespel A, Lerner-Natoli M. Angiogenesis is associated with blood–brain barrier permeability in temporal lobe epilepsy. Brain. 2007; 130:1942–1956. [PubMed: 17533168]

Rovati L, Salvatori G, Bulf L, Fonda S. Optical and electrical recording of neural activity evoked by graded contrast visual stimulus. Biomed. Eng. OnLine. 2007; 6:28. [PubMed: 17610733]

Seiffert E, Dreier JP, Ivens S, Bechmann I, Tomkins O, Heinemann U, Friedman A. Lasting blood–brain barrier disruption induces epileptic focus in the rat somatosensory cortex. J. Neurosci. 2004; 24:7829–7836. [PubMed: 15356194]

Seylaz J, Charbonne R, Nanri K, Von Euw D, Borredon J, Kacem K, Meric P, Pinard E. Dynamic in vivo measurement of erythrocyte velocity and flow in capillaries and of microvessel diameter in the rat brain by confocal laser microscopy. J. Cereb. Blood Flow Metab. 1999; 19:863–870. [PubMed: 10458593]

Shibasaki H. Human brain mapping: hemodynamic response and electrophysiology. Clin. Neurophysiol. 2008; 119:731–743. [PubMed: 18187361]

Shih AY, Friedman B, Drew PJ, Tsai PS, Lyden PD, Kleinfeld D. Active dilation of penetrating arterioles restores red blood cell flux to penumbral neocortex after focal stroke. J. Cereb. Blood. Flow Metab. 2009; 29:738–751. [PubMed: 19174826]

Stefanovic B, Hutchinson E, Yakovleva V, Schram V, Russell JT, Belluscio L, Koretsky AP, Silva AC. Functional reactivity of cerebral capillaries. J. Cereb. Blood Flow Metab. 2007; 28:961–972. [PubMed: 18059431]

Stoll G, Kleinschnitz C, Meuth SG, Braeuninger S, Ip CW, Wessig C, Nolte I, Bendszus M. Transient widespread blood–brain barrier alterations after cerebral photothrombosis as revealed by gadofluorine M-enhanced magnetic resonance imaging. J Cereb. Blood Flow Metab. 2008; 29:331–341. [PubMed: 18957988]

Strandgaard S, Paulson OB. Cerebral autoregulation. Stroke. 1984; 15:413–416. [PubMed: 6374982]

Strong AJ, Hartings JA, Dreier JP. Cortical spreading depression: an adverse but treatable factor in intensive care? Curr. Opin. Crit Care. 2007; 13:126–133. [PubMed: 17327732]

Tofts PS, Brix G, Buckley DL, Evelhoch JL, Henderson E, Knopp MV, Larsson HB, Lee TY, Mayr NA, Parker GJ, Port RE, Taylor J, Weisskoff RM. Estimating kinetic parameters from dynamic contrast-enhanced T(1)-weighted MRI of a diffusable tracer: standardized quantities and symbols. J. Magn. Reson. Imaging. 1999; 10:223–232. [PubMed: 10508281]

Tomita Y, Kubis N, Calando Y, Dinh AT, Meric P, Seylaz J, Pinard E. Long-term in vivo investigation of mouse cerebral microcirculation by fluorescence confocal microscopy in the area of focal ischemia. J. Cereb. Blood Flow Metab. 2005; 25:858–867. [PubMed: 15758950]

Tomkins O, Kaufer D, Korn A, Shelef I, Golan H, Reichenthal E, Soreq H, Friedman A. Frequent blood–brain barrier disruption in the human cerebral cortex. Cell. Mol. Neurobiol. 2001; 21:675–691. [PubMed: 12043841]

Tomkins O, Friedman O, Ivens S, Reiffurth C, Major S, Dreier JP, Heinemann U, Friedman A. Blood–brain barrier disruption results in delayed functional and structural alterations in the rat neocortex. Neurobiol. Dis. 2007; 25:367–377. [PubMed: 17188501]

Tomkins O, Shelef I, Kaizerman I, Eliushin A, Afawi Z, Misk A, Gidon M, Cohen A, Zumsteg D, Friedman A. Blood–brain barrier disruption in post-traumatic epilepsy. J Neurol. Neurosurg. Psychiatry. 2008; 79:774–777. [PubMed: 17991703]

van Vliet EA, da Costa AS, Redeker S, van SR, Aronica E, Gorter JA. Blood–brain barrier leakage may lead to progression of temporal lobe epilepsy. Brain. 2007; 130:521–534. [PubMed: 17124188]

Watson BD, Dietrich WD, Busto R, Wachtel MS, Ginsberg MD. Induction of reproducible brain infarction by photochemically initiated thrombosis. Ann. Neurol. 1985; 17:497–504. [PubMed: 4004172]

Zlokovic BV. The blood–brain barrier in health and chronic neurodegenerative disorders. Neuron. 2008; 57:178–201. [PubMed: 18215617]

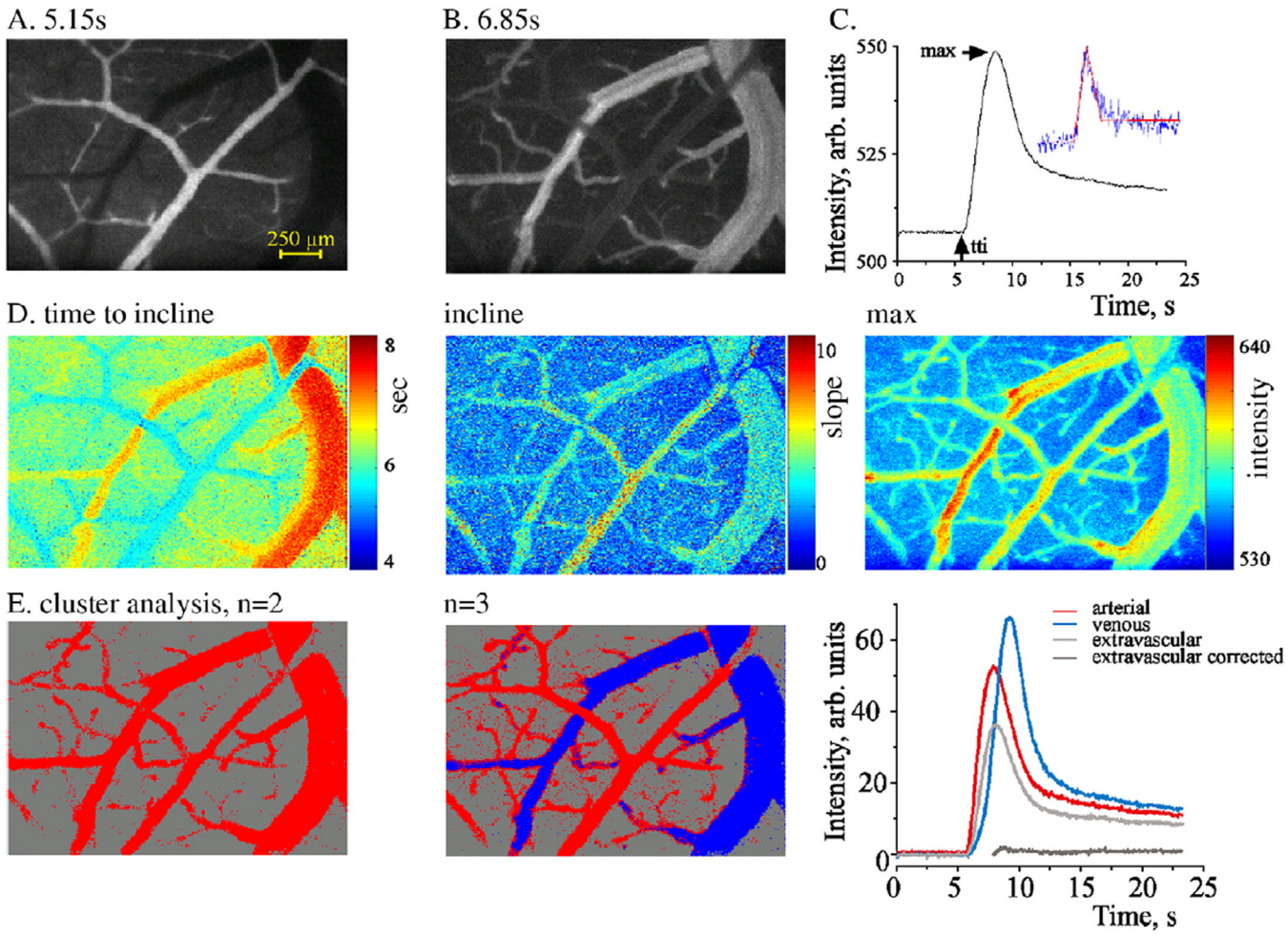

Fig. 1.

Flow visualization in pial vessels and image analysis: (A–C) Intravenous injection of the fluorescent tracer LY under control conditions resulted in an early increase in signal intensity within the surface arterioles (A), followed by delayed labeling of the venules (B). By using image analysis, an intensity–time curve was created (C), reflecting the change in tracer intensity within the local vasculature. The curve allows the estimation of several parameters using a segmented linear model (inset—red line, blue line—the raw data in a representative pixel). (D) Analysis results are represented for each voxel of the original image, enabling the distinction between defined vessels and the extravascular brain tissue. (E) Cluster analysis was used for automatic clustering of similarly behaving pixels (see Methods). Left image is the result of setting the number of clusters to 2; pixels are labeled as red for presumed blood vessels and gray for extravascular tissue. Right image—number of clusters was set to 3, allowing the distinction between arterioles (red), venules (blue) and tissue (gray). Light gray—the original signal in the extravascular compartment, dark gray—corrected signal following “background reduction” (see text).

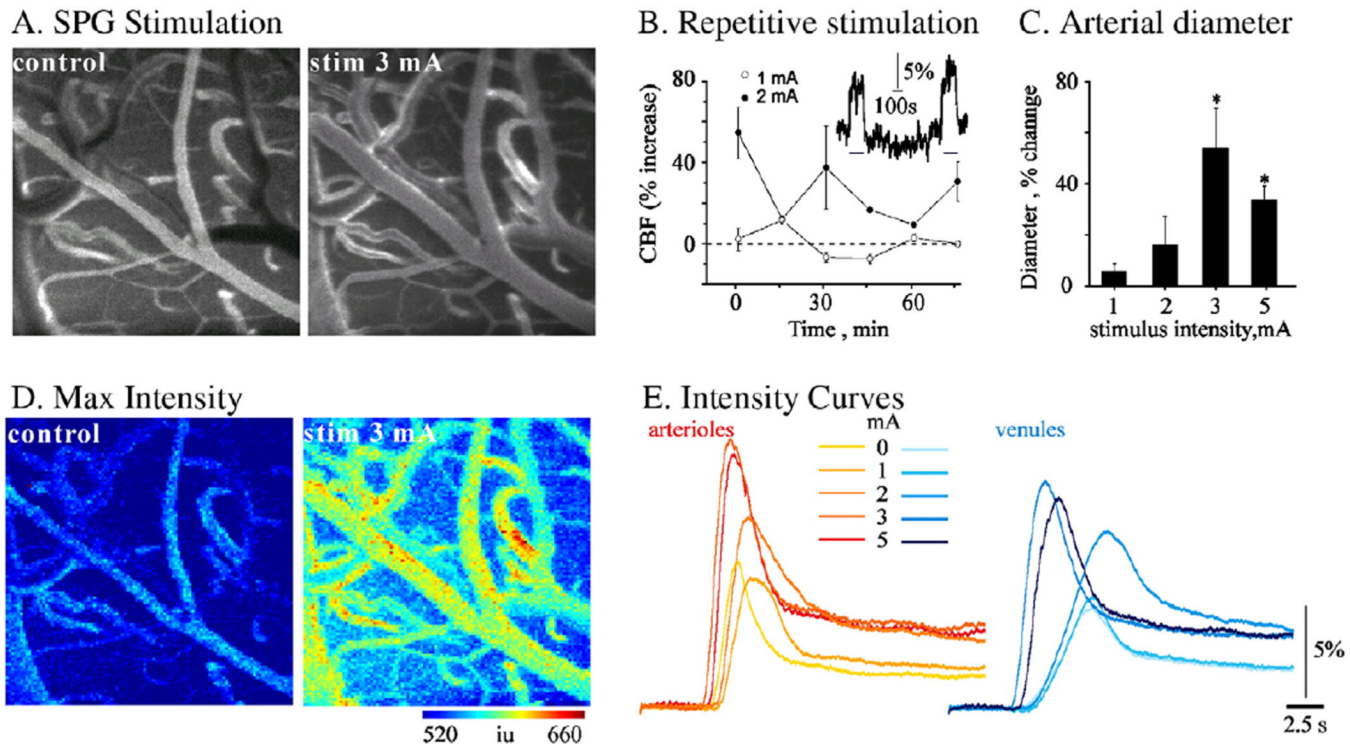

Fig. 2.

Experimental CBF increases following stimulation of the ethmoidal nerve: (A) A fluorescent tracer (LY) was injected under control conditions (left image) and at the end of each stimulus train (right image at 3 mA). Vasodilatation of surface vessels can clearly be seen. (B) LDF showed increased rCBF in each stimulation train above 1mA (inset). The graph shows mean measurements of maximal rCBF increase during each stimulation train, showing a consistent increase in mean rCBF when stimulation was repeated at 2 mA but not at 1mA ($n = 5$ at each intensity). (C) Stimulation of the ethmoidal nerve induced increase in rCBF, which was associated with intensity-dependent dilatation of arterioles. (D) Results of dynamic analysis during tracer injection are shown for *max* value, demonstrating an increasing change in maximal intensity (i.e., flow) following stimulation. (E) Mean intensity changes during injection in the arterial (left) and venous (right) compartments. Note that a significant reduction in *tti* and increases in *incline* and *max* values were observed at stimulation intensities higher than 1 mA.

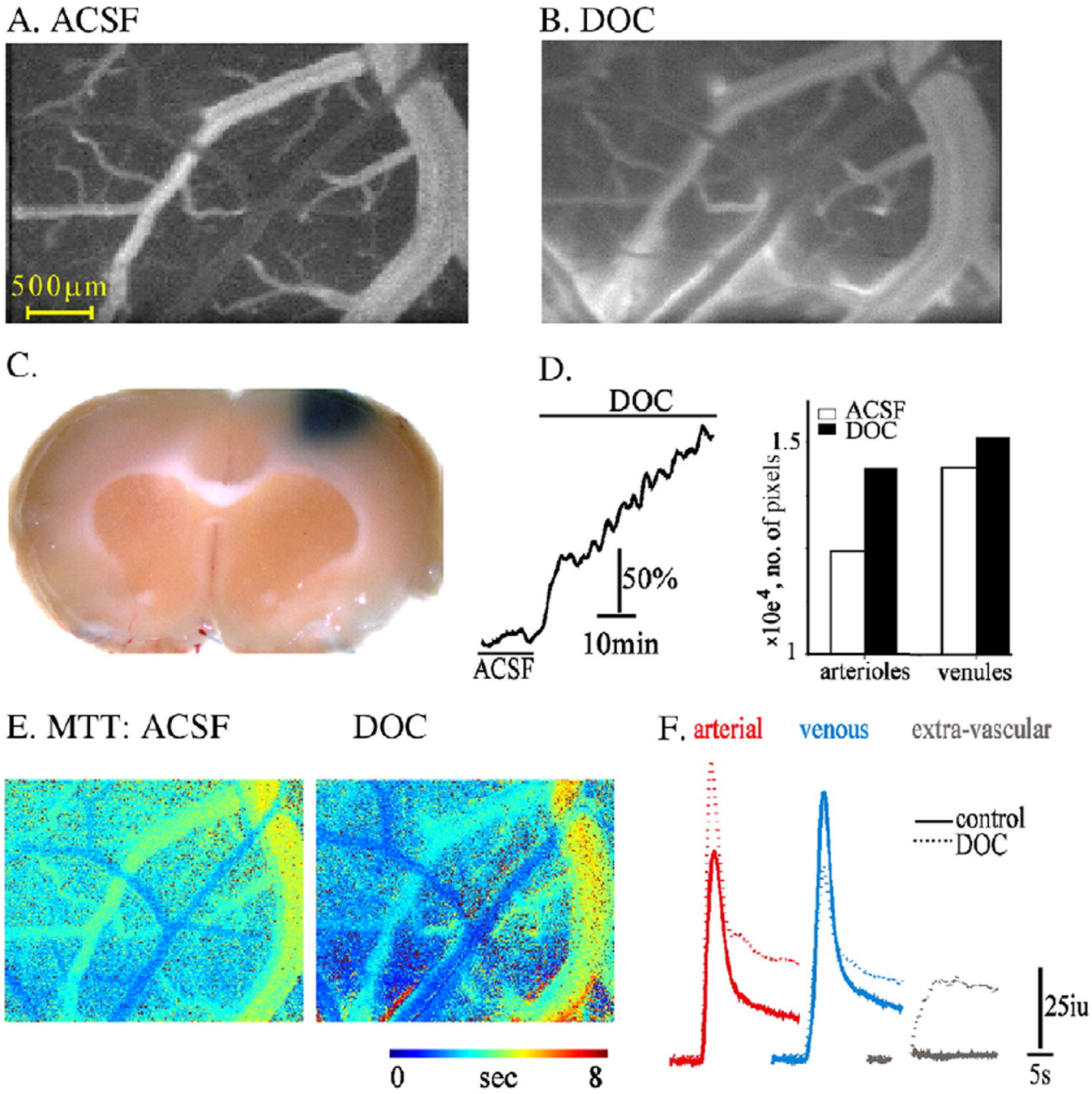

Fig. 3.

Imaging analysis reveals increased BBB permeability: (A–B) Fluorescent images of surface vessels during the venous phase of injection before (A) and after (B) DOC treatment. Diffusion of the injected tracer (LY) outside the vessels is seen after treatment, indicating BBB breakdown. (C) A coronal section following treatment with DOC and injection of Evans blue demonstrates extravasation of the albumin-binding dye into the treated cortical tissue, which indicates BBB breakdown. (D) Treatment with DOC was associated with a steady increase in LDF signal (left) and vasodilatation. The bar graph shows the number of pixels in the arterial and venous clusters under control conditions (ACSF) and following perfusion with DOC. (E) Maps of mean transient time (*MTT*) showing decreased *MTT* in

arterioles and the robust increase in the extravascular space where the tracer was accumulating. (F) Intensity curve for each compartment showing the increased flow in the arterial compartment together with decreased signal intensity in the venous compartment after DOC (dashed line). Note the robust slowing of the signal decay in the extravascular compartment after BBB breakdown.

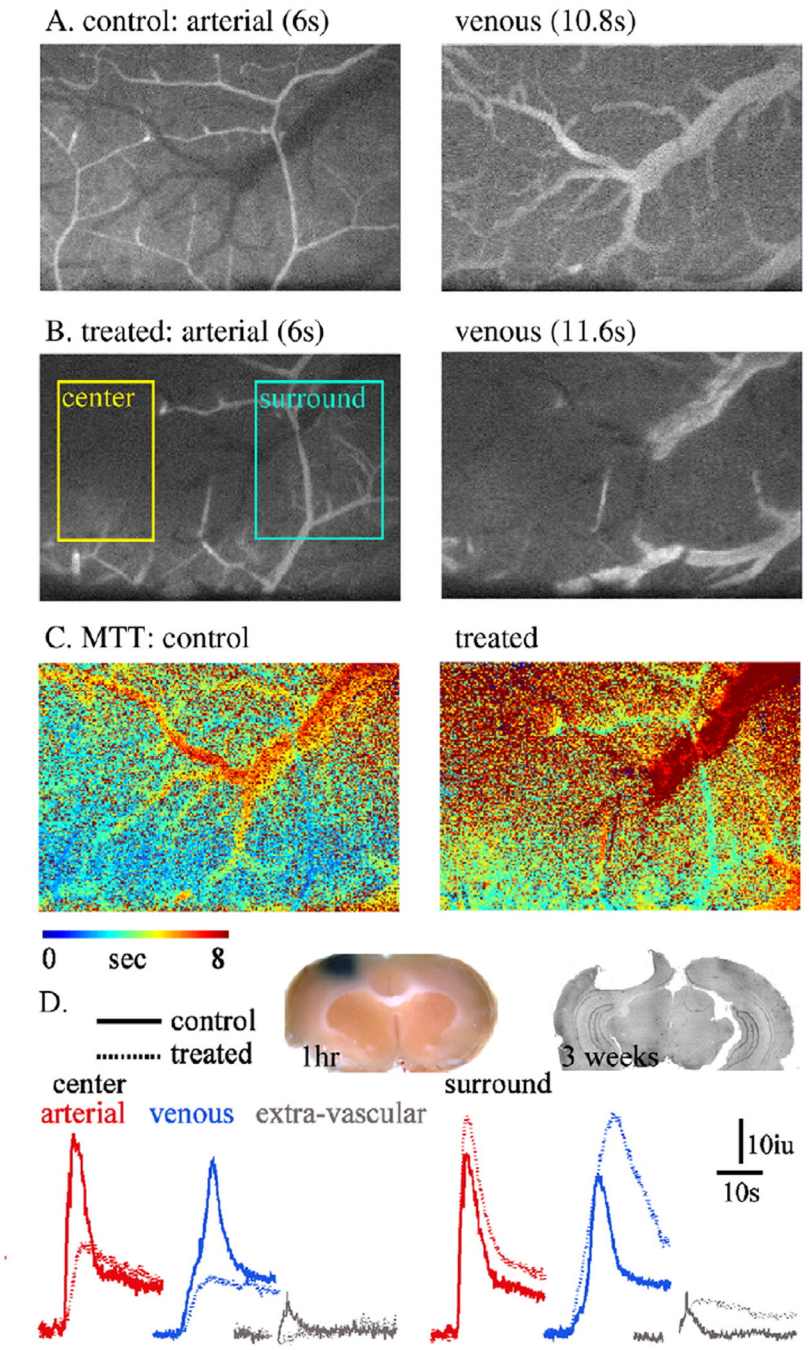

Fig. 4.

Intravascular thrombosis and experimental ischemia: (A, B) Fluorescent images of the arterial (left) and venous (right) phases before (A: control) and 30 min after (B) RBG injection and cortical exposure to light. The thrombotic vessels is observed as an abrupt stop of blood supply ("center"). Note the intact blood supply in the surrounding brain tissue ("surround"). (C) *MTT* maps before and after the induction of photo-thrombosis, showing the robust reduction in *MTT* in the ischemic region and the increased *MTT* in the surrounding ("penumbra"4) region. (D) Intensity curve for each compartment, showing the reduction in the perfusion in the ischemic core. In the surrounding brain a clear increase in signal is noted in the arterial, venous and extravascular compartments, suggesting increased

blood flow and BBB breakdown. Inset: left: brain tissue 1 h after RBG treatment (30 min after injection of Evans blue)—confirmed BBB breakdown in the region surrounding the thrombotic vessel. Right: histological brain section (cresyl violet staining) 21 days after a photothrombotic lesion.